INTERNATIONAL JOURNAL FOR NUMERICAL METHODS IN ENGINEERING
Int. J. Numer. Meth. Engng 2003; **57**:1737–1753 (DOI: 10.1002/nme.743)

A gradientless technique for optimal distribution of piezoelectric material for structural control

A. Mukherjee*,† and S. P. Joshi

Department of Civil Engineering, Indian Institute of Technology, Bombay, Mumbai 400076, India

SUMMARY

Application of *smart* piezoelectric materials in structural control is gaining momentum. Optimum placement and actuation of the smart material is an aspect of paramount importance in such structures. In this paper, we present an iterative technique to optimize the shape of piezoelectric actuators in order to achieve the desired shape of the structure. A C_0-continuous eight-node plate finite element with five degrees of freedom is employed. A gradientless shape design procedure based on the residual voltages is developed. It aims at minimizing the quadratic measure of the global displacement residual error between the desired and the current structural configuration. The actuators gradually adapt to a shape that is most efficient in resisting the external excitation. The present technique can be well suited for any static and time-varying excitation. In vibration control it is often necessary to create modal sensors and actuators in order to observe or excite some specific modes. Such modal sensors and actuators alleviate spillover problems and thus they avoid exhaustive signal processing. Several numerical examples for static as well as dynamic cases are presented to demonstrate the efficacy of the present technique.

KEY WORDS: smart materials; structural control; optimal transducer shapes; gradientless techniques; voltage residuals; modal transducers

1. INTRODUCTION

Recent technological advances in the field of material science, microelectronics and structural analysis and design have led to research in the development of high-performance structures that are light, energy efficient and autonomous, known as *smart structures*. These structures have embedded smart materials that are capable of sensing and controlling the changes in the structural characteristics. For example, studies are being conducted on integration of piezoelectric materials into aircraft wings in order to enhance their lift characteristics. Vibration suppression, shape control and instability control are some of the key applications of the smart structures technology. In precision structures like reflector antennas and deformable mirrors it

*Correspondence to: A. Mukherjee, Department of Civil Engineering, Indian Institute of Technology, Bombay, Mumbai 400076, India
†E-mail: abhijit@civil.iitb.ac.in

Received 19 April 2001
Revised 1 July 2002
Accepted 21 October 2002

is extremely vital to maintain their desired shape under the influence of external excitation. In the applications mentioned above controlled actuation is of paramount importance. The actuation can be controlled either by optimal distribution of the smart material or by optimal voltage distribution. In this paper, we demonstrate a technique for optimum shape design of sensors and actuators for the control of plate type structures.

Some reviews on controlled actuation are available (Padula and Kincaid [1] and Soares *et al.* [2]). The techniques for placement of sensors and actuators vary from intuitive recipes to numerical optimization techniques. Fripp and Atalla [3] carried out an extensive survey of modal sensing and actuation techniques. They highlighted the main characteristics, merits and limitations of different techniques e.g. physical shaping of continuous transducers and gain weighting of discrete transducers. Recently, Irschik [4] gave a general overview of the literature on shape control of structures under static and dynamic excitations. Gaudenzi and Barboni [5] determined the size and location of the discrete actuators by applying a number of constraints that uniquely define the design variables. However, this method requires artificial constraints to generate unique solutions. Barboni *et al.* [6] employed the pin-force model and the modal approach to obtain closed-form solutions for optimal size and location of actuators on beams under dynamic conditions. The beam deflection was expressed in terms of the mode shapes and modal co-ordinates that have the size and location of the actuator as the unknowns. Lee and Moon [7] developed a theory to derive modal sensors and actuators for one-dimensional structures using modal equations. They conducted experiments on a cantilever beam by fabricating mode 1 and mode 2 sensors. These modal sensors and actuators overcome spillover problems. However, the theory is difficult to apply to the structures with complex boundary conditions, as the closed-form solutions may not be available. Seeley and Chattopadhyay [8] solved a multiobjective optimization problem that includes discrete actuator location, vibration reduction, reduction in power consumption and maximization of fundamental frequency in the objective function. A non-linear constrained programming approach based on the method of feasible directions was employed in the solution of the cantilever box beams. Kapania *et al.* [9] used a heuristic integer programming approach to determine optimal locations of actuators in the control of thermal deformations of spherical mirror segments. Sun *et al.* [10] and Sun and Tong [11] designed discrete quasi-modal sensors and actuators by obtaining optimal locations and sizes of the predefined set of transducers. In their algorithm, they employed observation and control energy spillover criteria, respectively, for modal sensor and modal actuator design.

Several researchers have employed evolutionary algorithms in actuator placement problem. Onoda and Hanawa [12] used genetic (GA) and simulated annealing algorithms for optimal placement of actuators in shape control of space trusses. Gaudenzi *et al.* [13] demonstrated the use of GA in determining actuator distribution for beams. Zhang *et al.* [14] employed GA for sensor and actuator locations and the feedback gains simultaneously. The objective function was maximization of dissipation energy due to control action. The authors demonstrated the effectiveness of the GA over other conventional optimization technique in terms of computational efficiency and improvement in the solutions. Mukherjee and Joshi [15] have presented an iterative design procedure for determining actuator profiles for minimum power consumption.

Some researchers have used optimal voltage distribution in the control of the structures. Lin and Hsu [16] used sine-shaped sensors in the static control of beams. The voltage distribution in sensors and actuators are written in terms of the displacements and the general solution is

obtained using Fourier sine series. Agrawal and Treanor [17] presented analytical and experimental results on optimal placement of actuators and optimal voltages for beams. They developed an algorithm that optimized actuator placement and voltages for a given shape function. The authors reported that simultaneous optimization of actuator position and input voltages was unreliable due to the differences in the order of actuator locations and voltage terms in the optimization of cost function. Soares *et al.* [2] used higher-order finite-element models and gradient-based optimization techniques for optimal design of piezolaminated structures. The objective function was to maximize the piezoelectric actuator efficiency and minimize the weight of the structure. In the static shape control of plates the voltages were found out by minimizing the mean-squared error between the desired and actual transverse displacements. Chee *et al.* [18] devised a buildup voltage algorithm that is based on a high-order finite-element model for quasi-static shape control of plate structures. In this iterative approach, voltages on a few actuators with least error values are increased by a finite value and the process continues towards the determination of voltage profile over the plate.

In practice, control of structure using distributed voltages may require complicated electrical circuitry. Further, the voltage distribution technique is more amenable to quasi-static shape control and modal actuation than modal sensing. Moreover, discrete sensing and actuation is also limited by spatial aliasing in dynamic cases. Furthermore, using discrete actuators in shape control may lead to high stress gradients in localized zones. These problems could be overcome by designing spatially distributed transducers. We also note that most attempts at optimal sensing and actuation have been for beam structures. Optimization for actuator shapes for plate-type structures is scant. In beam structures it is possible to intuitively design the shape of the actuators and sensors that are very close to optimum. In case of plate structure an intuitive design is far more difficult, if not impossible. The present paper demonstrates a novel technique for the adaptive shape design of continuously distributed actuator and sensor profiles. The elegance of the present method is that it is universal, i.e. it can be applied for any structure with any form of external excitation. A gradientless procedure based on the residual voltages is developed. It aims at minimizing the quadratic measure of global displacement residual error between the desired and the current structural configuration. The actuators gradually adapt to a shape that is most efficient in controlling the structure. The present optimization technique is computationally economical and also avoids *checkerboard* designs that may be difficult to interpret and implement in practice.

2. MATHEMATICAL MODEL

2.1. Piezoelectricity equations

The piezoelectric material couples electrical energy with mechanical energy. The constitutive laws that govern this coupling are called as the direct and the converse piezoelectric effects. The constitutive relations for a piezolaminated plate is given by

$$\mathbf{D}_j = \mathbf{e}\boldsymbol{\varepsilon}_{ij} + \bar{\boldsymbol{\varepsilon}}\mathbf{E}_j \tag{1}$$

$$\boldsymbol{\sigma}_{ij} = \bar{\mathbf{D}}\boldsymbol{\varepsilon}_{ij} - \mathbf{e}^{\mathbf{T}}\mathbf{E}_j \tag{2}$$

where $\bar{\mathbf{D}}$ is the matrix of elastic constants, $\mathbf{e}$ the matrix of piezoelectric constants, $\bar{\boldsymbol{\varepsilon}}$ the matrix of dielectric constants, ε the mechanical strain vector, $\boldsymbol{\varepsilon}_{ij}$ is the mechanical strain of i-th surface in j-th direction, $\boldsymbol{\sigma}$ the stress vector induced by mechanical and electrical effects, $\mathbf{D}$ the electric displacement vector and $\mathbf{E}$ the electric field vector, $\mathbf{E}_j$ is the electric field strength in j th direction.

2.2. The displacement field

The displacement field of a laminated plate based on the first-order shear-deformation theory is given by

$$\begin{aligned} U(x,y,z,t) &= u_0 - z\theta_y(x,y,t) \\ V(x,y,z,t) &= v_0 + z\theta_x(x,y,t) \\ W(x,y,z,t) &= w_0(x,y,t) \end{aligned} \tag{3}$$

The terms u_0, v_0 and w_0 are the mid-plane displacements and θ_x and θ_y are the rotations of transverse normal about x- and y-axis. Using isoparametric relationships, the co-ordinates and displacements inside the element are defined as

$$x = \sum_{i=1}^{n} N_i x_i, \quad y = \sum_{i=1}^{n} N_i y_i, \quad u = \sum_{i=1}^{n} N_i \delta_i \tag{4}$$

where, N_i's are the element shape functions and n is the number of nodes per element. In the present work, an eight-node C_0-continuous plate element is employed in the analysis of piezolaminated plates.

2.3. Strain–displacement relation

The strain components at any point along the thickness of the plate are written in terms of strains at the reference plane as

$$\varepsilon = \begin{Bmatrix} \varepsilon_x \\ \varepsilon_y \\ \gamma_{xy} \\ \gamma_{yz} \\ \gamma_{xz} \end{Bmatrix} = \begin{Bmatrix} \dfrac{\partial U}{\partial x} \\ \dfrac{\partial V}{\partial y} \\ \dfrac{\partial U}{\partial y} + \dfrac{\partial V}{\partial x} \\ \dfrac{\partial W}{\partial y} + \theta_x \\ \dfrac{\partial W}{\partial x} - \theta_y \end{Bmatrix} = \begin{Bmatrix} \left(\dfrac{\partial u_0}{\partial x} - z\dfrac{\partial \theta_y}{\partial x}\right) \\ \left(\dfrac{\partial v_0}{\partial y} + z\dfrac{\partial \theta_x}{\partial y}\right) \\ \left(\dfrac{\partial u_0}{\partial y} - z\dfrac{\partial \theta_y}{\partial y}\right) + \left(\dfrac{\partial v_0}{\partial x} + z\dfrac{\partial \theta_x}{\partial x}\right) \\ \left(\dfrac{\partial w_0}{\partial y} + \theta_x\right) \\ \left(\dfrac{\partial w_0}{\partial x} - \theta_y\right) \end{Bmatrix} \tag{5}$$

Equation (3) can be written in concise form as

$$\boldsymbol{\varepsilon} = \mathbf{H}\bar{\boldsymbol{\varepsilon}} \tag{6}$$

where

$$\bar{\boldsymbol{\varepsilon}}^{\mathbf{t}} = \left(\frac{\partial u_0}{\partial x}, \frac{\partial v_0}{\partial y}, \left(\frac{\partial u_0}{\partial y} + \frac{\partial v_0}{\partial x}\right), \frac{\partial \theta_x}{\partial y}, -\frac{\partial \theta_y}{\partial x}, \left(\frac{\partial \theta_x}{\partial x} - \frac{\partial \theta_y}{\partial y}\right), \left(\frac{\partial w_0}{\partial y} + \theta_x\right), \left(\frac{\partial w_0}{\partial x} - \theta_y\right)\right) \quad (7)$$

$$\mathbf{H} = \begin{bmatrix} 1 & 0 & 0 & 0 & z & 0 & 0 & 0 \\ 0 & 1 & 0 & z & 0 & 0 & 0 & 0 \\ 0 & 0 & 1 & 0 & 0 & z & 0 & 0 \\ 0 & 0 & 0 & 0 & 0 & 0 & 1 & 0 \\ 0 & 0 & 0 & 0 & 0 & 0 & 0 & 1 \end{bmatrix} \quad (8)$$

The strains at the reference plane are related to the nodal displacements via strain–displacement matrix as follows:

$$\bar{\boldsymbol{\varepsilon}} = \mathbf{B}\boldsymbol{\delta}_{\mathbf{e}} \quad (9)$$

where

$$\boldsymbol{\delta}_{\mathbf{e}} = (u_0, v_0, w_0, \theta_x, \theta_y)^{\mathrm{t}} \quad (10)$$

$$\mathbf{B} = \sum_{r=1}^{n} \begin{bmatrix} \frac{\partial N_r}{\partial x} & 0 & 0 & 0 & 0 \\ 0 & \frac{\partial N_r}{\partial y} & 0 & 0 & 0 \\ \frac{\partial N_r}{\partial y} & \frac{\partial N_r}{\partial x} & 0 & 0 & 0 \\ 0 & 0 & 0 & \frac{\partial N_r}{\partial y} & 0 \\ 0 & 0 & 0 & 0 & -\frac{\partial N_r}{\partial x} \\ 0 & 0 & 0 & \frac{\partial N_r}{\partial x} & -\frac{\partial N_r}{\partial y} \\ 0 & 0 & \frac{\partial N_r}{\partial y} & N_r & 0 \\ 0 & 0 & \frac{\partial N_r}{\partial x} & 0 & -N_r \end{bmatrix} \quad (11)$$

2.4. Stress–strain relation

The laminated piezoelectric plate equations are obtained by integration of Equation (2) through the thickness

$$\begin{Bmatrix} \mathbf{N} \\ \mathbf{M} \end{Bmatrix} = \bar{\mathbf{D}} \begin{Bmatrix} \varepsilon \\ \kappa \end{Bmatrix} - \begin{Bmatrix} \mathbf{N^P} \\ \mathbf{M^P} \end{Bmatrix}; \quad \begin{Bmatrix} \mathbf{Q}_x \\ \mathbf{Q}_y \end{Bmatrix} = \begin{bmatrix} \mathbf{S_{44}} & \mathbf{S_{45}} \\ \mathbf{S_{54}} & \mathbf{S_{55}} \end{bmatrix} \begin{Bmatrix} \gamma_{xz} \\ \gamma_{yz} \end{Bmatrix} \tag{12}$$

where

$$\bar{\mathbf{D}} = \int \mathbf{H^t Q H}\, \mathrm{d}z \tag{13}$$

$\mathbf{N^P}$ and $\mathbf{M^P}$ are the generalized stress resultants due to piezoelectric effects and $\mathbf{Q}_x$ and $\mathbf{Q}_y$ are the shear stress resultants. The piezoelectric stress resultants are derived in the following section.

2.5. Actuator and sensor mechanics

If the voltage is applied to the piezoelectric layer only in the thickness direction, the electric field intensity $(E_3)^k$ in the equation is expressed as

$$(E_3)^k = \frac{V^k}{h^k} \tag{14}$$

where, V^k is the applied voltage across k-th layer and h^k is the thickness of k-th layer.

The actuator force and moment resultants written in Equation (12) are given as

$$\begin{Bmatrix} \mathbf{N}_x^{\mathbf{P}} & \mathbf{M}_x^{\mathbf{P}} \\ \mathbf{N}_y^{\mathbf{P}} & \mathbf{M}_y^{\mathbf{P}} \\ \mathbf{N}_{xy}^{\mathbf{P}} & \mathbf{M}_{xy}^{\mathbf{P}} \end{Bmatrix} = \sum_{k=1}^{N\text{lay}} \int_{z(k-1)}^{z(k)} \begin{Bmatrix} \mathbf{e_{31}} \\ \mathbf{e_{32}} \\ \mathbf{0} \end{Bmatrix}^k \{1, z\}(E_3)^k\, \mathrm{d}z \tag{15}$$

The actuator nodal force vector is obtained as

$$\mathbf{F^P} = \iint_A \mathbf{B^T} \begin{Bmatrix} \mathbf{N^P} \\ \mathbf{M^P} \end{Bmatrix} \mathrm{d}A \tag{16}$$

According to the Gauss law, the closed circuit charge (q) measured through the electrodes of a sensor patch in k-th layer is

$$q = \frac{1}{2} \left(\left[\int_R D_3^k\, \mathrm{d}A \right]_{z=z_k} + \left[\int_R D_3^k\, \mathrm{d}A \right]_{z=z_{k-1}} \right) \tag{17}$$

As the charge is collected only in the thickness direction, the dielectric displacement in direction 3 only is of interest. Moreover, it can be assumed that for a piezoelectric layer acting as a sensor, electric field in direction 3 is zero. Thus, Equation (1) is modified as

$$D_3^k = \mathbf{e}\boldsymbol{\varepsilon} \tag{18}$$

Substituting Equations (2) and (9) in the above equation we get

$$q = \int_R (\mathbf{eB}\boldsymbol{\delta}_\mathbf{e})\,\mathrm{d}A \tag{19}$$

The sensor voltage is computed as

$$V_\mathrm{s} = \frac{q}{C} \tag{20}$$

where, C is the capacitance of the piezoelectric material.

3. SENSOR AND ACTUATOR SHAPE DESIGN

In this section, we present the iterative algorithm for adaptive design of sensor and actuator profiles. The present design method can be applied for static as well as dynamic cases. In static analysis the objective is to determine the actuator profile that would be efficient in obtaining the desired shape of the structure after it has deformed under external forces. In dynamic analysis the sensor or the actuator configurations corresponding to the mode shapes that are to be observed or excited are determined. It is to be noted that a reciprocal relationship exists between the sensor and the actuator. Therefore, the shape of the sensor that observes a particular mode (modal sensor) is also the shape of the actuator that excites that mode (modal actuator). The present iterative procedure can therefore be employed in designing both modal sensors and actuators. The objective is to minimize the quadratic measure of the residual deviation of the current deformations of the structure from its desired state. The objective function is thus defined as

$$\min \left[\int \{\boldsymbol{\delta}_\mathbf{i}(p_1, A_1, \ldots, p_n, A_n) - \boldsymbol{\delta}_\mathbf{0}\}^2 \,\mathrm{d}A \right] \tag{21}$$

where δ_i is the normalized deformation vector in i-th iteration, $A_i, \ldots, A_n$ the areas of actuators that are switched on, $(p_1, \ldots, p_n)$ the actuator position vector and δ_0 the normalized desired deformation vector.

The step-by-step procedure for the solution is described below:

1. The entire structural domain is discretized using a fine finite-element mesh.
2. In case of static analysis the deformation vector is the solution obtained after analysing the structure for external mechanical loads. In the dynamic analysis the mode shape for which the sensor/actuator profile is to be obtained is the deformation vector. Using sensor relation (Equation (20)), the voltage in each element (V_s^e) is calculated.
3. The shape design process begins with a maximal *seed* design in that all actuators switched on. The process continues towards shape determination by *killing* the undesired actuators. To begin the process of removal of actuators a novel concept of *front opening* is implemented (Figure 1). The front is defined by the physical boundaries of the structure. The actuators that lie on the front are removed from the locations of minimal absolute curvature. This is termed as front opening. The actuators that surround the front are candidates for state change.
4. The structure is analysed based on the current actuator configuration under unit voltage and the voltages developed due to current actuator configuration are calculated (V_a^e).

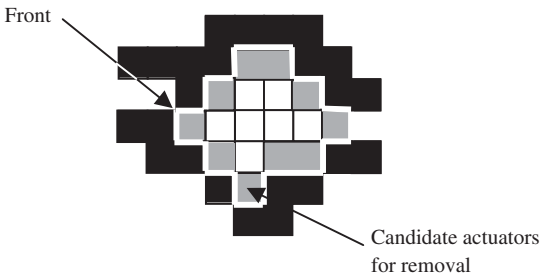

Figure 1. Front growth.

Table I. Material properties.

Property	PVDF	Aluminium
Young's modulus (GPa), E_1, E_2	2.0, 2.0	70.0
Poisson's ratio, v_{12}	0.30	0.25
Shear modulus (GPa), G_{12}	0.775	28.00
Piezoelectric strain constant, C/m^2, $e_{31} = e_{32}$	-0.046	—
Thickness (mm)	0.50	0.50
Number of layers	2 (each at top and bottom)	2 (between the piezoelectric layers)
Mass density ($N\,s^2/m^4$)	1800	2700

5. The voltages V_a^e and V_s^e are normalized with respect to their maximum values.

$$\bar{V}_s^e = \frac{V_s^e}{(V_s^e)_{max}}; \quad \bar{V}_a^e = \frac{V_a^e}{(V_a^e)_{max}} \tag{22}$$

The residual voltages (V_r^e) for the elements on the front are determined as

$$V_r^e = (\bar{V}_s^e - \bar{V}_a^e) \tag{23}$$

The elements that have negative residuals are potential actuators to be removed. In practice, a predetermined fraction of these actuators are removed.

6. The quadratic measure of the global residual deviation (α) in deformation is calculated as

$$\alpha = \sum_{i=1}^{ndof} (\boldsymbol{\delta_i} - \boldsymbol{\delta_0})^2 \tag{24}$$

7. Steps 4–6 are repeated until the value of α is acceptably small.

4. NUMERICAL RESULTS AND DISCUSSION

In this section, we present the results for both static as well as dynamic cases. Table I contains the properties of the plate and the piezoelectric material for all the examples.

4.1. Static analysis

In the first three examples we consider plates with large aspect ratios that can be treated as one-dimensional structures. The actuator profiles for these structures under given external load can be determined by physical intuition or by hand calculations. Subsequently, a plate with smaller aspect ratio is considered to investigate the two-dimensional case.

Example 1 (*A cantilever plate subjected to edge load*). A long cantilever plate, ($0.1\,\mathrm{m} \times 0.02\,\mathrm{m}$), is subjected to a unit edge load. The objective is to find out the actuator layout that gives the original undeformed shape under the given load. Using symmetric boundary conditions, only half the structure is modelled with a 75×7 finite-element (FE) mesh. The piezoelectric effect e_{32} is neglected in order to compare the result with one-dimensional solutions. Of the total number of actuators that lie on the front, two actuators that satisfy the condition (Equation (23)) explained in the design procedure are removed in each iteration. Figures 2(a)–2(d) show the actuator configurations at different stages of the design process. The optimal shape for the problem is shown in Figure 2(d). The method produces a design that is very close to the optimal shape. The histories of the global displacement and the global residual voltage errors are shown in Figure 3. The global residual error in displacement shows a smoother variation in comparison to the global error in voltage. The voltages are dependent on the strains in the structure, which are obtained by differentiating displacements. Thus, any small variation in displacement history reflects significantly in the voltage curve. Therefore, the global displacement error is superior to the global voltage error as a convergence criterion.

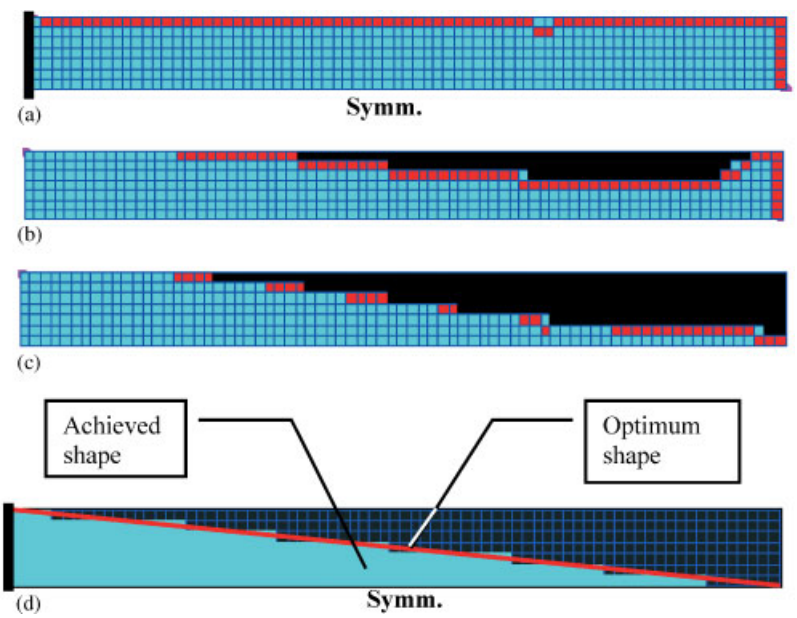

Figure 2. Actuator design history (example 1): (a) seed design; (b) fifty iterations; (c) one hundred iterations; and (d) final design.

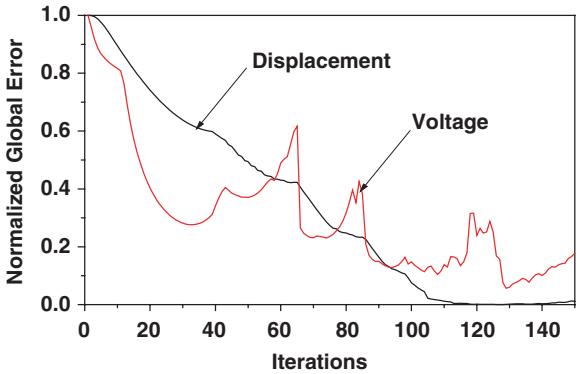

Figure 3. Error history (Example 1).

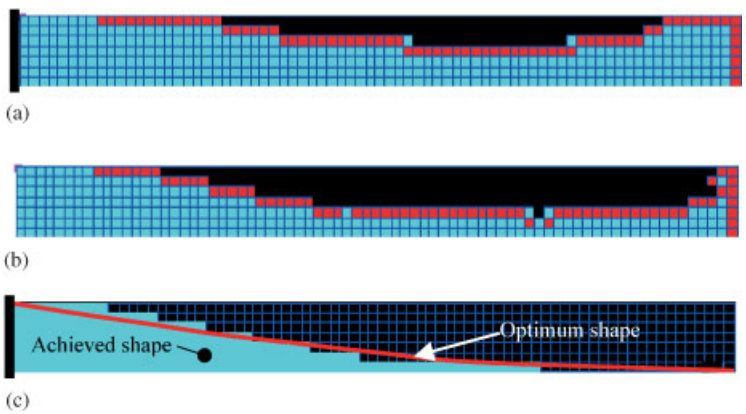

Figure 4. Actuator design history (Example 2): (a) fifty iterations; (b) one hundred iterations; and (c) final design.

Example 2 (*A cantilever plate subjected to uniform pressure*). The plate in Example 1 is subjected to a uniform pressure. The objective is to find out the optimum actuator layout in order to obtain the original undeformed configuration. The piezoelectric effect e_{32} is neglected. Two actuators from the front that satisfy the requirement are removed in each iteration. Figures 4(a)–4(c) show the different stages in the actuator shape determination. The global error in displacement reduces monotonically till the minimum value is reached (Figure 5). Beyond this point any further removal leads to increase in the error.

Example 3 (*A simply supported long plate subjected to uniform pressure*). The boundary conditions for the plate in the first example are modified and the plate is simply supported at two short edges. The plate is subjected to a unit pressure and the actuator profile to regain the original undeformed configuration is determined (Figures 6(a)–6(c)). Like the previous two

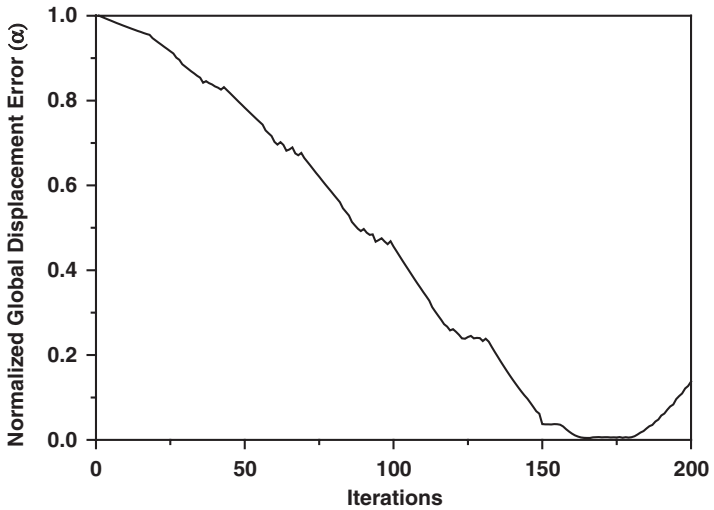

Figure 5. Error history (Example 2).

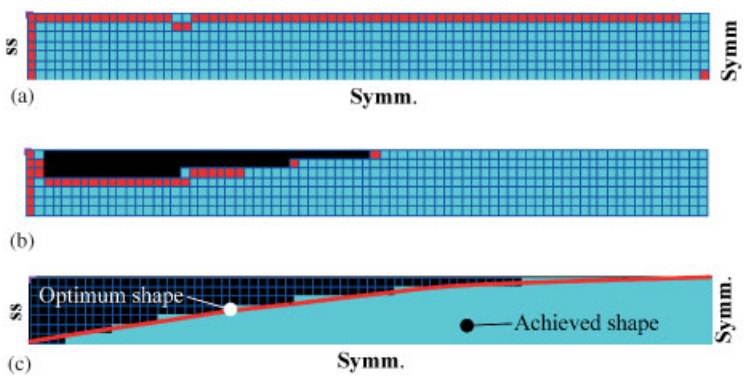

Figure 6. Actuator design history (Example 3): (a) seed design; (b) forty iterations; and (c) final design.

examples, the piezoelectric effect e_{32}, is neglected. Figure 7 shows the convergence history of the design.

Example 4 (*A simply supported rectangular plate subjected to uniform pressure*). In the previous examples the plates with large aspect ratio were considered. The piezoelectric effect in the shorter direction was neglected so that the results could be compared with one-dimensional solutions. In this example, we consider a plate with smaller aspect ratio ($0.2\ \text{m} \times 0.1\ \text{m}$), simply supported at all four edges. The plate is subjected to uniform unit pressure. The piezoelectric effects in both the directions are important. The effect of actuator removal rate is also studied in this example. In the first case two actuators of the possible candidate actuators are removed in each iteration (Figures 8(a)–8(d)). In the second case four actuators are

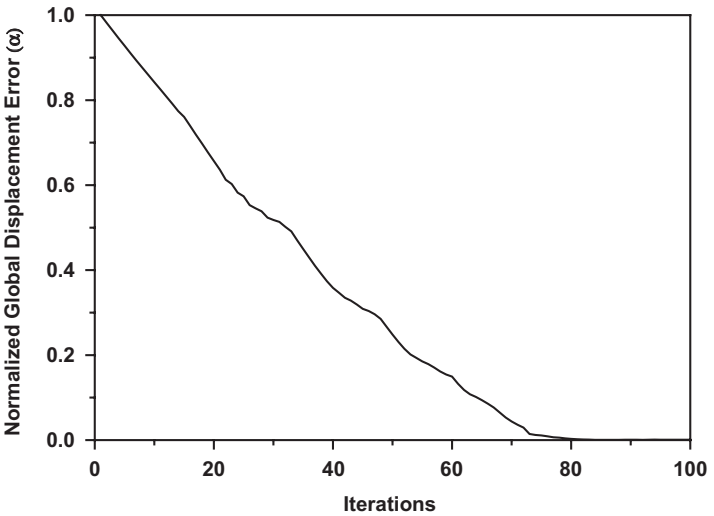

Figure 7. Error history (Example 3).

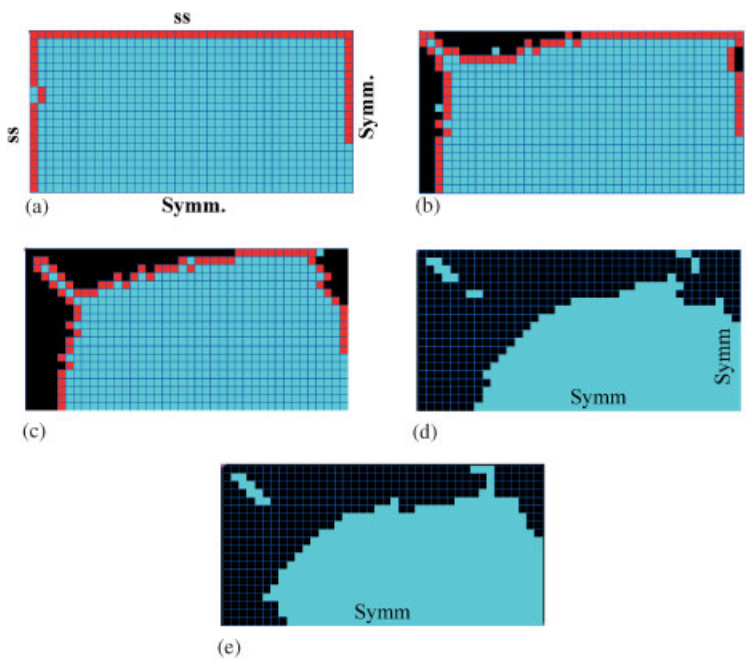

Figure 8. Actuator design history (Example 4): (a) seed design; (b) forty iterations; (c) eighty iterations; (d) final design (case I); and (e) final design (case II).

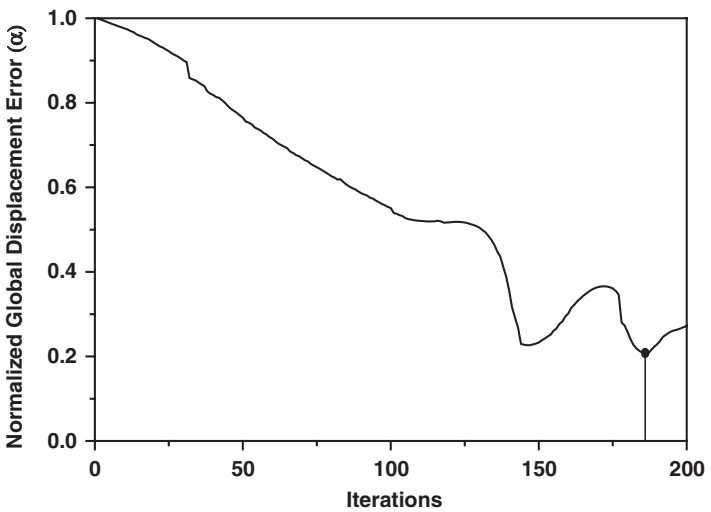

Figure 9. Error history (Case I, Example 4).

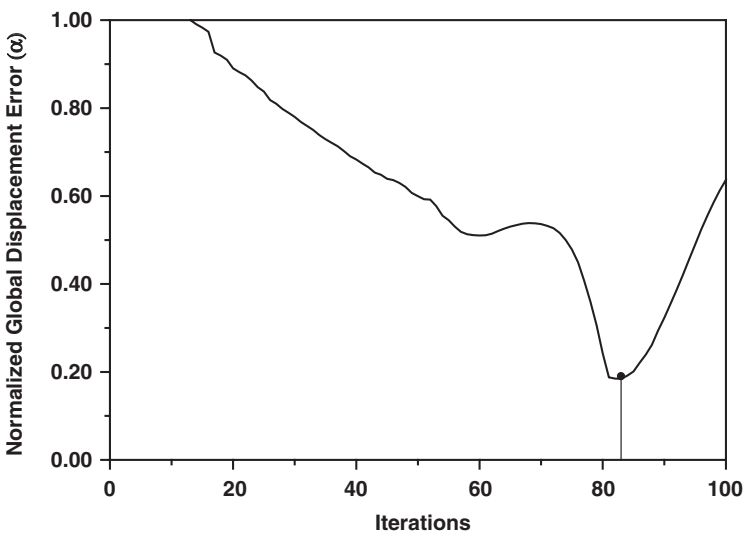

Figure 10. Error history (Case II, Example 4).

removed in each iteration (Figure 8(e)). It is seen that the two cases produce similar design with minor differences. The global displacement error curves (Figures 9 and 10) also show similar trends. The higher actuator removal rate has the advantage of being computationally faster. The error curves highlight an important aspect of the present design procedure. The solution successfully crosses the local minima and proceeds to reach the global minimum.

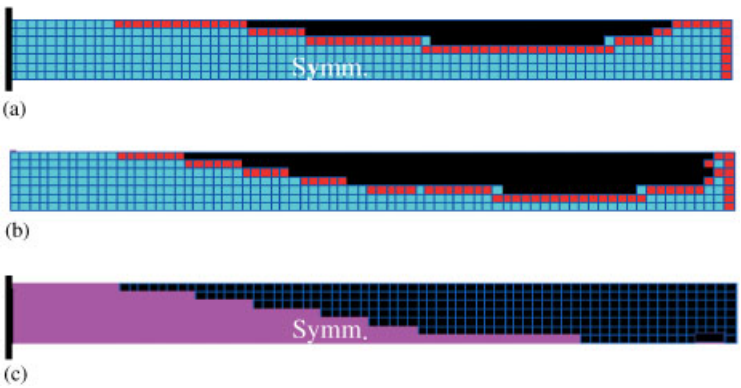

Figure 11. Design history for sensor optimized for mode 1 (Example 5): (a) fifty iterations; (b) one hundred iterations; and (c) final design.

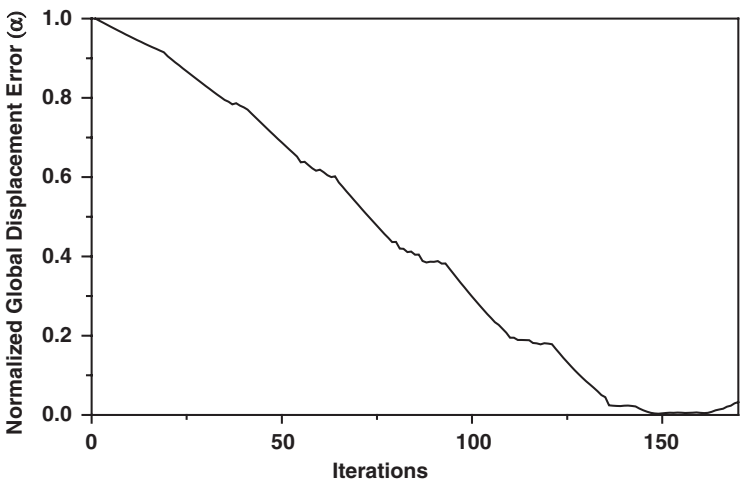

Figure 12. Error history (Example 5).

4.2. *Dynamic analysis*

The applicability of the present design technique to obtain the sensor profiles corresponding to the modes that are to be observed is investigated in this section. The mode shape is used to determine the optimum sensor profile that would respond to the desired mode. These sensors are termed as modal sensors as they would detect only those natural frequencies for which they are designed.

Example 5 (*A long cantilever plate*). The first two natural frequencies and the corresponding mode shapes for the cantilever plate in Example 1 are obtained by free vibration analysis. The mode shapes are then fed to the optimization routine. In both the cases the piezoelectric effect in the shorter direction is neglected. Figures 11(a)–11(c) show the intermediate and

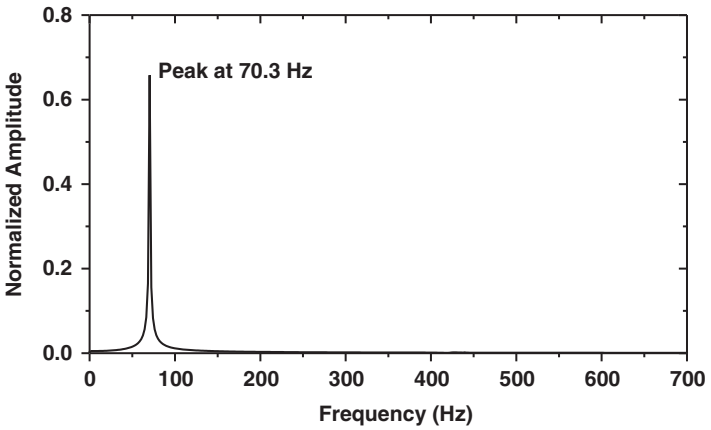

Figure 13. Response of mode 1 sensor corresponding to external excitation (Example 5).

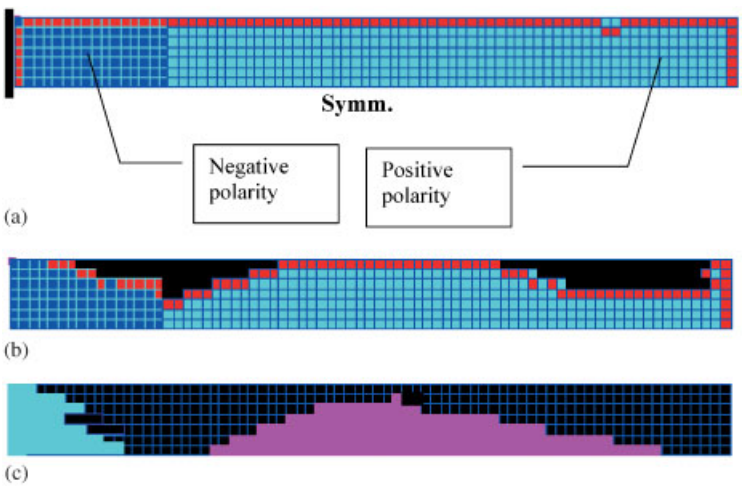

Figure 14. Design history for sensor optimized for mode 2 (Example 5): (a) seed design; (b) fifty iterations; and (c) final design.

final sensor profiles corresponding to the first mode and Figure 12 shows the global displacement error history. To examine the efficacy of the sensor design, the structure is subjected to external excitation of nature $f = f_0\ (A \sin \omega_1 t + B \sin \omega_2 t)$, where A and B are the constants and ω_1 and ω_2 are the forcing frequencies close to the first two natural frequencies of the system. A fast Fourier transform of the signal generated by the sensor optimized for the first mode (Figure 13) shows only one peak at the first frequency. Thus, the sensor filters out the second mode successfully.

Figures 14(a)–14(c) show the sensor profiles at various stages of the design process for the second mode. Owing to changing curvature, the sensors have opposite polarities on either side of the line of contraflexure. Figure 15 shows the history of global displacement error. The efficacy of the sensor shape is found out by using this shape in detecting the signal from

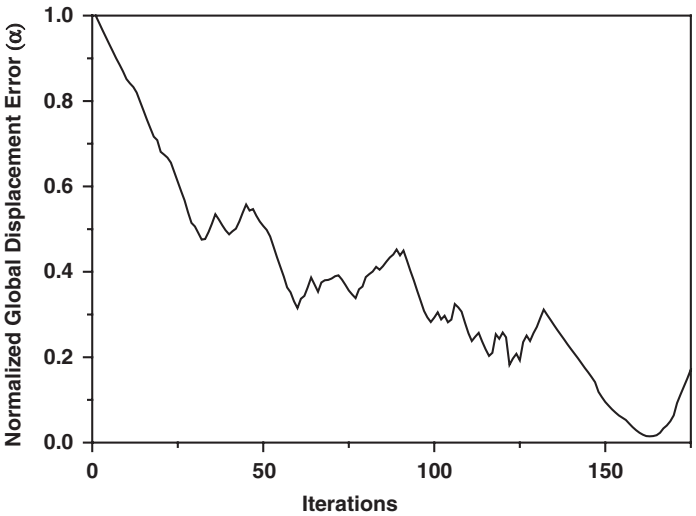

Figure 15. Error history (Example 5).

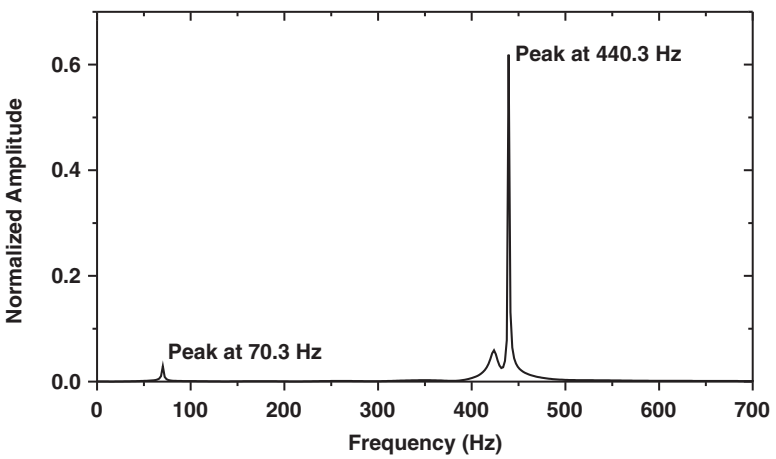

Figure 16. Response of mode 2 sensor corresponding to external excitation (Example 5).

the system under the influence of the forcing function described earlier. It is seen from Figure 16 the sensor optimized for mode 2 responds predominantly in the second mode.

5. CLOSING REMARKS

In this paper, a gradientless technique to optimize the distribution of piezoelectric sensors and actuators for efficient control of plates has been presented. The present design procedure is simple and can easily be integrated into existing finite-element tools. A novel concept of front has been developed that makes the design process computationally faster as only

the sensors/actuators on the front are the candidates for state change. It also eliminates the checkerboard patterns of the sensors/actuators, which are difficult to interpret. The method is universal; i.e. it can be applied to any structure with any external excitation. Several numerical examples demonstrate the efficacy of the design procedure. It is also shown that modal sensors and actuators can be constructed using the present design technique.

REFERENCES

1. Padula SL, Kincaid RK. Optimization strategies for sensor and actuator placement. *NASA Technical Memorandum TM*-1999-209126, 1999.
2. Soares CMM, Soares CAM, Correia VMF. Optimal design of piezolaminated structures. *Composite Structures* 1999; **47**:625–634.
3. Fripp ML, Atalla MJ. Review of modal sensing and actuation techniques. *Shock and Vibration Digest* 2001, **33**(1):3–14.
4. Irschik H. A review on static and dynamic shape control of structures by piezoelectric actuation. *Engineering Structures* 2002; **24**:5–11.
5. Gaudenzi P, Barboni R. Static adjustment of beam deflections by means of induced strain actuators. *Smart Materials and Structures* 1999; **8**:278–283.
6. Barboni R, Mannini A, Fantini E, Gaudenzi P. Optimal placement of PZT actuators for the control of beam dynamics. *Smart Materials and Structures* 2000; **9**:110–120.
7. Lee CK, Moon FC. Modal sensors/actuators. *Transactions of ASME* 1990; **57**:434–441.
8. Seeley CE, Chattopadhyay A. The development of an optimization procedure for the design of intelligent structures. *Smart Materials and Structures* 1993; **2**:135–146.
9. Kapania RK, Mohan P, Jakubowski A. Control of thermal deformations of spherical mirror segment. *Journal of Spacecraft and Rockets* 1998; **35**(2):156–162.
10. Sun D, Tong L, Wang D. Vibration control of plates using discretely distributed piezoelectric quasi modal actuators/sensors. *AIAA Journal* 2001; **39**(9):1766–1772.
11. Sun D, Tong L. Modal control of smart shells by optimized discretely distributed piezoelectric transducers. *International Journal of Solids and Structures* 2001; **38**:3281–3299.
12. Onoda J, Hanawa Y. Actuator placement optimization by genetic and improved simulated annealing algorithms. *AIAA Journal* 1993; **31**(6):1167–1169.
13. Gaudenzi P, Enrico F, Koumousis V, Gantes C. Genetic algorithm optimization for the active control of a beam by means of PZT actuators. *Journal of Intelligent Materials Systems and Structures* 1998; **9**:291–300.
14. Zhang H, Lennox B, Goulding P, Leung A. A float-encoded genetic algorithm technique for integrated optimization of piezoelectric actuator and sensor placement and feedback gains. *Smart Materials and Structures* 2000; **9**:552–557.
15. Mukherjee A, Joshi SP. Design of actuator profiles for minimum power consumption. *Smart Materials and Structures* 2001; **10**(2):305–313.
16. Lin CC, Hsu CY. Static shape control of smart beam plates laminated with sine sensors and actuators. *Smart Materials and Structures* 1999; **8**:519–530.
17. Agrawal BN, Treanor KE. Shape control of a beam using piezoelectric actuators. *Smart Materials and Structures* 1999; **8**:729–740.
18. Chee C, Tong L, Steven G. A buildup voltage (BVD) algorithm for shape control of smart plate structures. *Computational Mechanics* 2000; **26**(2):115–128.

